arXiv:cond-mat/0104297v1 [cond-mat.mes-hall] 17 Apr 2001

Numerical Renormalization Group Analysis of Interacting Quantum Dots

Walter Hofstetter

Theoretische Physik III, Elektronische Korrelationen und Magnetismus,
Universität Augsburg, 86135 Augsburg

Abstract. Wilson's Numerical Renormalization Group (NRG) is so far the only nonperturbative technique that can reliably access low–energy properties of quantum impurity systems. We present a recent extension of the method, the DM–NRG, which yields highly accurate results for dynamical quantities at arbitrary frequencies and temperatures. As an application, we determine the spectrum of a quantum dot in an external magnetic field. Furthermore, we discuss magnetic impurities with orbital degeneracy, which have been inferred in recent experiments on quantum dots in an Aharonov-Bohm geometry. It is demonstrated that for spinless electrons, interference between neighbouring levels sets the low–energy scale of the system. Switching on an external field leads to a remarkable crossover into a regime dominated by *orbital* Kondo screening. We predict that the broadening–induced level splitting should be clearly visible in measurements of the optical absorption power. A more general model including the electron spin is studied within an extended two-band NRG procedure. We observe competition between interference and Kondo screening, similar to the situation in two-impurity models (RKKY).

1 Introduction

Quantum impurity models and their low-temperature properties are of central importance in condensed matter physics. They show characteristic many-body effects like the screening of a local moment by conduction electrons (the Kondo effect) which was first observed in measurements on dilute magnetic impurities in metals (see [1]). More recently, artificial nanostructures (quantum dots [2] or surface atoms probed by STM [3,4]) with tunable parameters provided new representations of the Anderson or Kondo model [5,6]. In theory, a very fruitful line of research was opened by the development of dynamical mean-field theory (DMFT) [7] where correlated lattice systems are mapped onto effective impurity models which are then accessible in a controlled way [8].

In this article, we focus on semiconductor nanostructures, where – at the moment – experiments with the highest level of control can be performed. Electronic transport through ultra-small quantum dots, where the charging energy is the largest energy scale, has been studied extensively over the last few years [9]. Due to the quantization of charge the transport is dominated by Coulomb blockade. More recently, experiments revealed that the Kondo

effect leads to an enhancement of the conductance – the *zero bias anomaly* – in the Coulomb blockade regime [2,10] as predicted some time ago [11].

Theoretical modelling of these systems is usually based on the Kondo or Anderson Hamiltonians [5,6] describing a localized spin (orbital) which is coupled to one or several conduction electron reservoirs. In the regime of interest, this coupling is the usually the smallest energy scale. It was realized very early [6] that a treatment of these models based on perturbation theory fails due to logarithmic divergences below a characteristic temperature scale, the *Kondo temperature* T_K.

Solution of the Kondo problem at $T \ll T_K$ thus required a *non–perturbative* technique, which was provided by Wilson's pathbreaking *Numerical Renormalization Group* (NRG) [12]. It proved to be very successful in clarifying the low–energy properties of various impurity problems [13,14,15,16,17], and it will be the method of choice for analyzing more complex quantum dot systems.

In this article we give a short introduction to the NRG technique, including in particular a recently developed density–matrix formalism (the DM–NRG [18]) necessary for a reliable calculation of dynamical quantities. Using the new algorithm, impurity spectra are calculated for a quantum dot in an external magnetic field. Finally, we discuss the subtle interplay between interference and interaction which arises in a quantum dot with orbital degeneracy.

2 Generalized Numerical Renormalization Group

In the following, we consider the Anderson Hamiltonian [5]

$$H_{\rm and} = \sum_{\mathbf{k}\sigma} \epsilon_{\mathbf{k}}\, c^\dagger_{\mathbf{k}\sigma}\, c_{\mathbf{k}\sigma} + \sum_{\mathbf{k}\sigma} V_{\mathbf{k}} \left(f^\dagger_\sigma\, c_{\mathbf{k}\sigma} + h.c. \right) + U\, n_{f\uparrow}\, n_{f\downarrow} + \epsilon_f\, n_f - h\, S^z_f \quad (1)$$

where the *hybridization* $\Gamma(\omega) = 2\pi \sum_k |V_k|^2\, \delta(\omega - \epsilon_k)$ between the f impurity and the reservoir electrons $c_{\mathbf{k}\sigma}$ is balanced by a local Coulomb repulsion U which suppresses double occupancy of the impurity. In addition, a local magnetic field h is coupled to the impurity spin S^z_f. Units are chosen as $\hbar = k_B = \mu_B = g = 1$ and the half bandwidth is given by $D = 1$.

The key idea introduced by Wilson is the *logarithmic discretization* of the conduction band shown in Fig. 1, where each energy scale is represented by a single fermionic degree of freedom. After performing a Lanczos transformation (for details see [12,19]) the conduction band can be written as a linear chain shown in Fig. 2

$$H_{\rm and} = \sum_{\substack{n=0 \\ \sigma}}^{\infty} \epsilon_n \left(d^\dagger_{n\sigma}\, d_{(n+1)\sigma} + h.c. \right) \quad (2)$$

with hopping coefficients decaying *exponentially* as $\epsilon_n \sim \Lambda^{-n/2}$. In this representation, the impurity is only coupled to the *maximally localized* reservoir

state $d_0 = (1/\sqrt{N})\sum_k c_k$. The transformed model – while still a nontriv-

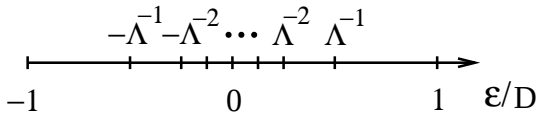

Fig. 1. Logarithmic discretization of the conduction band.

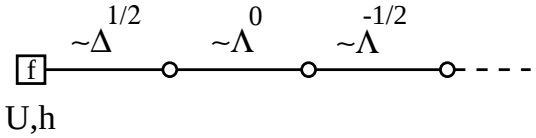

Fig. 2. Linear chain representation of the Anderson impurity Hamiltonian.

ial many–body problem – can now be solved by iterative diagonalization, keeping in each step only the lowest, most relevant levels. This procedure resembles the one employed in calculating atomic spectra and is illustrated in Fig. 3. Additional symmetries like the conservation of the total charge and components of the total spin can be invoked in order to simplify the remaining matrix algebra. In the single–band case considered here, matrix size is not a problem, while for calculations with two (different) reservoirs the use of symmetries can be vital in order to render the problem manageable.

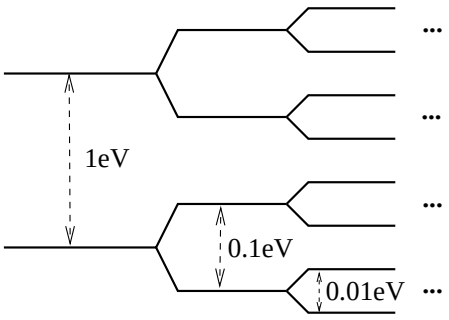

Fig. 3. Iterative diagonalization of the impurity problem.

In the iterative diagonalization scheme, the number of iterations corresponds to the temperature one is interested in according to $T_N = c\,\Lambda^{-(N-1)/2}$,

where c is a constant of order one. For calculating static thermodynamic expectation values, all necessary information is thus obtained because only excitations on the scale T_N are relevant. As an example, consider the impurity magnetization

$$< S_f^z >_T = Z^{-1} \sum_m e^{-\beta E_m^N} \; < m|S_f^z|m >_N \tag{3}$$

where the $|n>$ are the many-particle eigenstates of H and Z is the partition function. Due to the Boltzmann factor, higher excitations – already lost in iteration N – can be safely neglected at this point.

The situation changes completely when we consider a *dynamical* quantity like the spin–resolved spectral density

$$A_\sigma(\omega) = \sum_{nm} | < m|f_\sigma^\dagger|n > |^2 \, \delta \left(\omega - E_m + E_n\right) \, \frac{e^{-\beta E_m} + e^{-\beta E_n}}{Z}. \tag{4}$$

Obviously, spectral information at frequencies $\omega \gg T_N$ requires matrix elements between low-lying states and excitations which in iteration N are not available anymore (they have already been lost by truncation). In order to deal with this situation, the following *two–stage* procedure has to be employed:

(1) NRG iterations are performed down to the temperature T_N of interest, in particular we choose $T_N \ll T_K$ to calculate ground-state properties. In each iteration step, we keep the information on the transformation between one set of eigenstates and the next, i.e. we save the corresponding unitary matrix. After obtaining the relevant excitations at temperature T_N one can define the density matrix

$$\hat{\rho} = Z^{-1} \sum_m e^{-E_m^N/T_N} \; |m >_N < m| \tag{5}$$

which completely describes the physical state of the system. The equilibrium Green's function can be written as

$$G_\uparrow(t) = i\theta(t) \mathrm{Tr} \left(\hat{\rho} \, \left\{ f_\uparrow(t), f_\uparrow^\dagger(0) \right\} \right) \tag{6}$$

(2) Now we repeat the iterative diagonalization for the same parameters. Each iteration step N' yields the single-particle excitations (and matrix elements of $f^\dagger$) relevant at a frequency $\omega \sim T_{N'}$. But instead of using (4), we now employ (6) and evaluate the spectral function with respect to the correct *reduced density matrix* [20]: As depicted in Fig. 4, the complete chain is split into a smaller cluster of length N' and an *environment* containing the remaining degrees of freedom. In the product basis of these two subsystems, the full density matrix has the form

$$\hat{\rho} = \sum_{\substack{m_1 m_2 \\ n_1 n_2}} \rho_{m_1 n_1, m_2 n_2} |m_1 >_{\mathrm{env}} \, |n_1 >_{\mathrm{sys}} < n_2| < m_2| \tag{7}$$

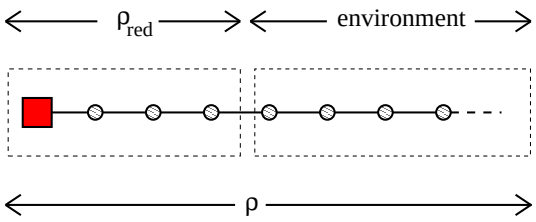

Fig. 4. Reduced density matrix obtained by tracing out "environment" degrees of freedom of the chain.

which is in general not diagonal anymore. Performing a partial trace on the environment then yields the density submatrix

$$\hat{\rho}^{\rm red} = \sum_{n_1 n_2} \rho^{\rm red}_{n_1 n_2} |n_1 >_{\rm sys} < n_2| \quad , \quad \rho^{\rm red}_{n_1 n_2} = \sum_m \rho_{m n_1, m n_2} \tag{8}$$

This projection is easily done using the previously stored unitary transformation matrices. Note that $\rho^{\rm red}$ – defined only on the shorter chain – contains all the relevant information about the quantum mechanical state of the *full* system.

The single–particle spectrum calculated in this way is shown in Fig. 5. With increasing magnetic field, the Kondo resonance is suppressed and eventually merges with the lower atomic level. Regarding the total density of states (DOS) $A(\omega) = \sum_\sigma A_\sigma(\omega)$, the Kondo peak is split by the field and the DOS at the Fermi level strongly reduced. This effect has been observed directly in measurements of the differential conductance through a quantum dot [2].

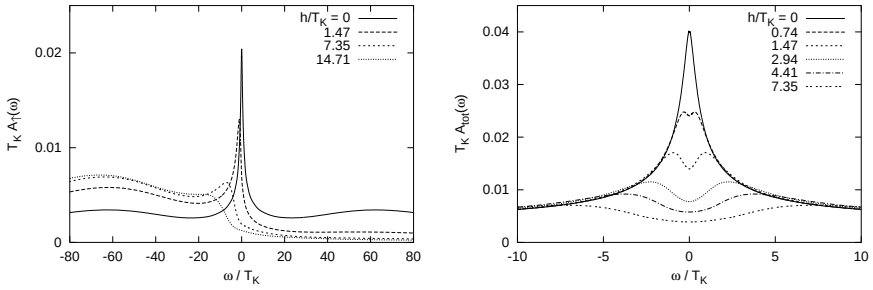

Fig. 5. Spin–dependent (left) and total (right) impurity spectral density at zero temperature for $\Gamma = 0.02$, $U = 5\Gamma$, and $\epsilon_f = -2.5\Gamma$. The Kondo temperature is $T_K = 6.8 \times 10^{-4}$.

3 Interference and Interaction in Multi–Level Dots

After the discussion of the spin–degenerate Anderson impurity model (1) in the last section, we now consider the effect of *orbital* degeneracy. We will first study a dot consisting of two levels without spin or, equivalently, two dots in an Aharonov-Bohm (AB) geometry with one level per dot in the presence of an interdot Coulomb repulsion U. Such a system is of fundamental interest since the two possible paths through the dot (via level 1 or 2) can interfere with each other. The interference can be controlled by an AB flux and has attracted much interest due to the possibility of realizing AB interferometers [22] or using the coherent properties in connection with quantum computing [23]. Furthermore, there is enhanced experimental interest to study quantum dots in the strong tunneling regime where the level broadening is of the order of the level spacing. In this case, transport is inevitably controlled by multi-level physics.

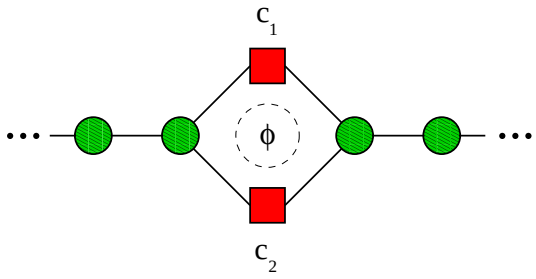

Fig. 6. Two quantum dots in an Aharonov–Bohm geometry.

Let us first discuss the case of *spinless* electrons, assuming e.g. a large Zeeman splitting [24]. The Hamiltonian is then written as

$$H = \sum_{kr} \varepsilon_{kr} a_{kr}^\dagger a_{kr} + \sum_{rkj} (V_j^r a_{kr}^\dagger c_j + \text{h.}c.) + \sum_j \varepsilon_j c_j^\dagger c_j + U n_1 n_2 \tag{9}$$

where $j = 1, 2$ labels the two levels and the dot is connected to two reservoirs $r = L, R$ via tunnel barriers. Note that the index labelling the dots is not present in the reservoirs – this model contains no conserved quantum number corresponding to spin, unlike previous studies [25,26,27,28]. The tunnel matrix elements are assumed to be real except for an AB-phase, i.e. we attach a phase factor $e^{i\phi}$ to V_2^L. The level broadening is defined by $\Gamma_j^r = 2\pi |V_j^r|^2 \rho_0$, where ρ_0 is the density of states in the leads, which we assume to be constant in the energy range of interest. The total broadening of each level is therefore given by $\Gamma = \Gamma_j^L + \Gamma_j^R$.

Since both levels overlap with the reservoirs, they have an effective overlap matrix element Δ, which induces a level splitting $\delta\tilde{\epsilon} = \sqrt{\delta\epsilon^2 + |\Delta|^2}$ where

$\delta\epsilon = \epsilon_2 - \epsilon_1$ denotes the bare level spacing. Within second–order perturbation theory it is established that Δ vanishes for the noninteracting dot, while

$$\Delta \sim \frac{\sqrt{\Gamma_1^R \Gamma_2^R} + \sqrt{\Gamma_1^L \Gamma_2^L} e^{i\phi}}{\pi} \ln\left(U/\omega_c\right) \tag{10}$$

in the case of strong on–site repulsion $U \gg |\epsilon|, \Gamma$. For positive level energies, the tunnel splitting can be observed directly as a shift of the upper level position (see Fig. 7) in the total spectral density

$$A(\omega) = -\frac{1}{\pi} \sum_{i,j=1,2} \mathrm{Im} G_{ij}(\omega^+). \tag{11}$$

For low lying levels $\epsilon < -\Gamma$ and a large Coulomb repulsion, the dot is singly occupied at low temperatures. In this case, the effective level splitting shows up in a many-body resonance ("shoulder") in the spectral density at a *positive* frequency $\omega \sim \delta\tilde{\epsilon}$, see Fig. 7. This new many–body energy scale can

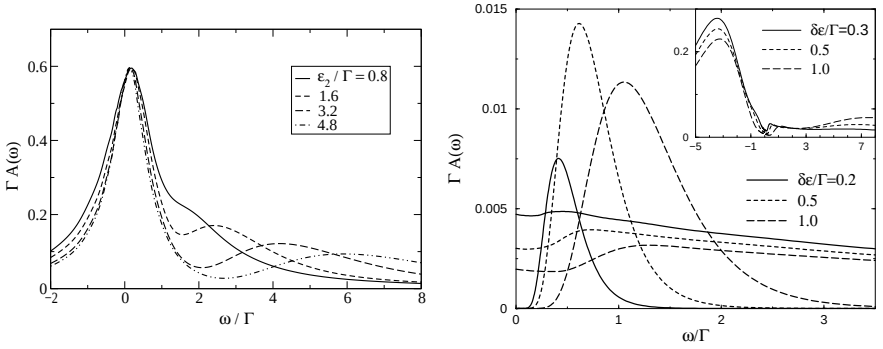

Fig. 7. Left: tunnel splitting visible in the total spectral function for parameters $U = 16\Gamma$, $\epsilon_1 = \Phi = T = 0$ and different positions of the second levels ϵ_2. Right: Absorption power (broken lines) vs. single–particle spectral density (full lines) for $U = 50\Gamma$, $\epsilon_1 = -10\Gamma$ and $\Phi = T = 0$. In the inset, $U = 10\Gamma$ and $\epsilon_1 = -3.5\Gamma$ [24].

be seen most clearly in a microwave absorption experiment, where transitions between the two dot levels are induced due to the dipole operator $\hat{O} = c_1^\dagger c_2 + c_2^\dagger c_1$. The corresponding spectral density

$$\rho_{\mathrm{abs}}(\omega) = Z^{-1} \sum_{mn} |< n|\hat{O}|m >|^2 \, \delta\left(\omega + E_n - E_m\right) \left(e^{-\beta E_n} - e^{-\beta E_m}\right) \tag{12}$$

displays a well–pronounced resonance at the frequency $\delta\tilde{\epsilon}$ (see Fig. 7).

For $\phi = \pi$ and $\Gamma_j^R = \Gamma_j^L$, the tunnel splitting is zero, and the system is shown to be equivalent to an Anderson model with Zeeman splitting $\delta\epsilon$. This can be seen most easily by introducing the new levels

$$c_{\mathrm{even(odd)}} = (1/\sqrt{2})(c_1 \pm c_2) \tag{13}$$

which are then coupled to the right and left reservoirs, respectively. In this way, an *orbital* Kondo effect can be realized in a quantum dot even in the absence of an *a priori* conserved quantum number like spin. The crossover between the interference– and Kondo–dominated regimes upon increase of the AB–phase ϕ is most clearly seen in the single particle spectrum (Fig. 8) where the Kondo resonance gradually develops as $\phi \to \pi$. Experimentally, the absorption power may be more easily accessible: With increasing ϕ, the absorption maximum is shifted from $\delta\tilde{\epsilon}$ to $\min(T_K, \delta\epsilon)$, while at the same time the absorption intensity strongly increases (see Fig. 8).

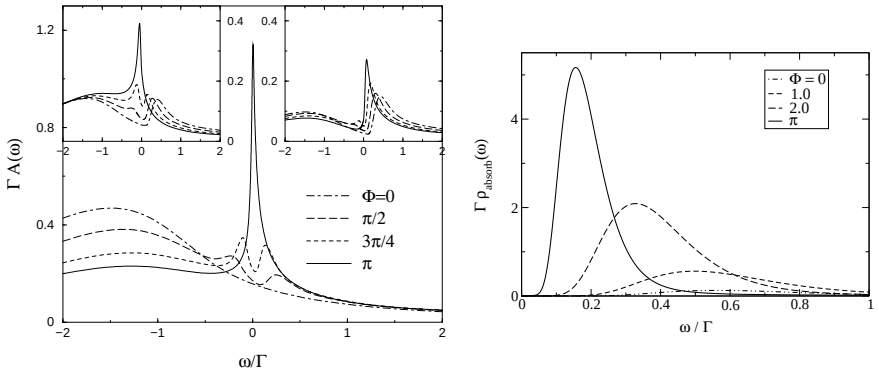

Fig. 8. Left: Effect of the AB–phase ϕ on the single–particle spectrum. The total spectral density is shown for $\epsilon_1 = -1.6\Gamma$, $\delta_\epsilon = 0$, $U = 8.1\Gamma$, and $T = 0$. Insets: Partial spectral densities for levels c_1 (left) and c_2 (right). Same parameters as above, but with a finite level splitting $\delta\epsilon = 0.08\Gamma$. Right: Absorption power for $U = 33\Gamma$, $\epsilon_1 = -3.3\Gamma$, $\delta\epsilon = 0.16\Gamma$, $T = 0$ and different values of ϕ.

So far, we have assumed that both levels are equally broadened by the reservoir, i.e. $\Gamma_1 = \Gamma_2$. In experiments, this need not be the case, although tuning within $\delta\Gamma = 20\%$ seems feasible. In order to clarify whether the *orbital* Kondo effect discussed previously is still visible under these conditions, we have therefore determined the influence of an asymmetric broadening on the single particle spectrum (Fig. 9). In the Kondo regime $\phi \approx \pi$ our model then corresponds to an effective Anderson Hamiltonian with spin–dependent hybridization, which is interesting in itself and has not been studied before. For the parameters used, we find a robust Kondo peak, which is split, but remains clearly visible even at an asymmetry of $\delta\Gamma = 100\%$. We therefore conclude that the orbital Kondo effect discussed here should be accessible under realistic experimental conditions.

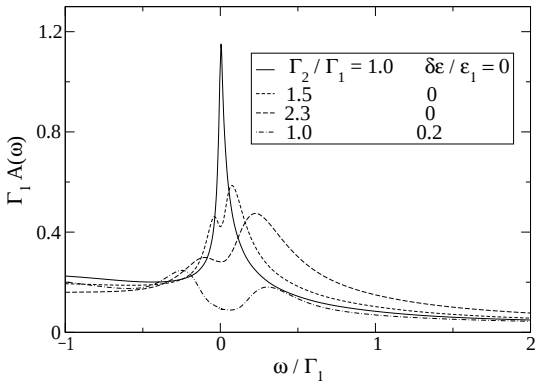

Fig. 9. Effect of an asymmetric broadening of the two levels for $U = 16.2\Gamma_1$, $\epsilon_1 = -3.2\Gamma_1$, $\Phi = \pi$, $T = 0$ and different values of Γ_2. For comparison, the influence of a finite level splitting is also shown.

Finally, we would like to extend our model to include the electron spin, which should give rise also to a *magnetic* Kondo effect. In this case, the dot Hamiltonian has to be generalized as

$$H_{\rm dot} = \sum_j \varepsilon_j c^\dagger_{j\sigma} c_{j\sigma} + U n_1 n_2 + U_1 n_{1\uparrow} n_{1\downarrow} + U_2 n_{2\uparrow} n_{2\downarrow} \tag{14}$$

where $n_i = \sum_\sigma n_{i\sigma}$. For the special case of $U = U_1 = U_2$ and $\delta\epsilon = 0$, this model has been studied before [27,28]. In realistic double–dot systems, however, we expect $U < U_{1,2}$. This is the parameter regime we will address here.

NRG calculations for the model including spin are very expensive from a computational point of view. This is due to the larger size of the conduction band Hilbert space, which now contains four instead of two additional fermionic degrees of freedom per iteration, as shown in Fig. 10. In our calcu-

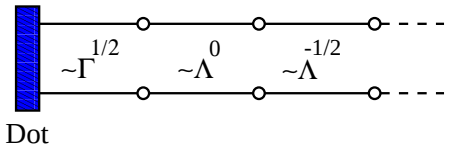

Fig. 10. Effective NRG Hamiltonian for the spin–degenerate dot (14).

lations, we kept about up to 1000 levels in each iteration step, which for 20 iterations required about 10 hours of CPU time on an IBM Power 3.

Results are shown in Fig. 11: For vanishing AB–phase ϕ, the two dot levels are coupled to the same reservoir. The resulting RKKY interaction [29] leads to an effective ferromagnetic exchange coupling between the levels. For zero interdot correlation ($U = 0$), the resulting side peaks dominate the single–particle spectrum (left plot). In addition, the screening of the total dot spin leads to the Kondo resonance at the Fermi level, which is suppressed for increasing broadening Γ.

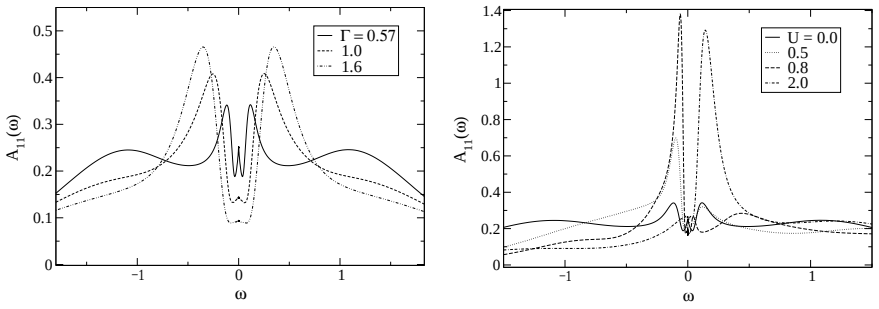

Fig. 11. Partial spectral density for level c_1 of a spin–degenerate double quantum dot. Left: $U = 0$, $U_1 = U_2 = 2.0$, $\epsilon_1 = \epsilon_2 = -1.0$ and $\Phi = T = 0$ with varying Γ. Right: Same parameters, but now $\Gamma = 0.61$ is fixed and the interdot interaction U is tuned to different values.

Switching on the interdot U as shown in the right plot of Fig. 11 enhances the lower side peak. At $U = 1$, a discontinuous change in the ground state occupation number occurs, while at even larger values of U, one again obtains the interference "shoulder" already discussed in the spinless case.

For a finite AB–phase ϕ we expect interplay of the *orbital* and *magnetic* Kondo effects, which will be the subject of a future publication [30].

4 Conclusion

In this paper we have discussed Wilson's Numerical Renormalization Group, a powerful nonperturbative method designed specifically to calculate low–temperature properties of quantum impurity systems. It is the only method that yields reliable results for systems with very different energy scales (small Kondo temperature T_K, large bandwidth). Recent experimental progress in the fabrication of ultrasmall quantum dots has made the preparation of artificial Kondo "atoms" with well–controlled parameters possible. NRG is the method of choice for the theoretical interpretation of spectral and transport measurements in terms of single impurity models.

We have presented an extended NRG algorithm (DM–NRG) suitable for calculating low–temperature dynamics in the full frequency range. This

method has been applied to calculate the spectrum of a quantum dot in a magnetic field.

Furthermore, we have studied the interplay between interference and Kondo correlations in multi–level quantum dots. *Orbital* Kondo screening has been observed which can be tuned by an external Aharonov–Bohm phase and should be most easily visible in the optical absorption power. Additional spin degeneracy gives rise to the (Spin–) Kondo effect and causes an effective RKKY–interaction between the two dot levels. We expect competition between magnetic and orbital screening in the presence of a finite AB–phase. These results should be useful for the interpretation of recent experiments on vertically coupled dots (see e.g. [31]) or lateral multi–dot arrangements [32].

In future applications of the NRG method, more complex impurities will be considered – one may even try to model the lowest exitations of a complete molecule in order to describe recent transport experiments, see e.g. [33]. From the methodical point of view, the extension of NRG to non–equilibrium calculations remains a major challenge.

The author would like to thank R. Bulla, H. Schoeller, and D. Vollhardt for valuable discussions. This work was supported by the Deutsche Forschungsgemeinschaft through SFB 484.

References

1. A.C. Hewson, *The Kondo Problem to Heavy Fermions*, (Cambridge University Press, 1993).
2. D. Goldhaber-Gordon *et al.*, Nature **391**, 156 (1998); S.M. Cronenwett *et al.*, Science **281**, 540 (1998); J. Schmid *et al.*, Phys. Rev. Lett. **84**, 5824 (2000). W. G. van der Wiel *et al.*, Science **289**, 2105 (2000).
3. J. Li, W.-D. Schneider, R. Berndt, and B. Delley, Phys. Rev. Lett. **80**, 2893 (1998).
4. H.C. Manoharan, C.P. Lutz, and D.M. Eigler, Nature **403**, 512 (2000).
5. P.W. Anderson, Phys. Rev. **B 124**, 41 (1961).
6. J. Kondo, Prog. Theor. Phys. **32**, 37 (1964).
7. W. Metzner and D. Vollhardt, Phys. Rev. Lett. **62**, 324 (1989).
8. A. Georges, G. Kotliar, W. Krauth, and M.J. Rozenberg, Rev. Mod. Phys. **68**, 13 (1996).
9. *Mesoscopic Electron Transport*, eds. L.L. Sohn *et al.*, (Kluwer, 1997); *Single Charge Tunneling*, eds. H. Grabert and M.H. Devoret, (Plenum Press, 1991); D.V. Averin and K.K. Likharev, in *Mesoscopic Phenomena in Solids*, ed. B.L. Altshuler, (Elsevier, 1991).
10. F. Simmel *et al.*, Phys. Rev. Lett. **83**, 804 (1999).
11. L.I. Glazman and M.E. Raikh, Sov. Phys. JETP Lett. **47**, 452 (1988); T.K. Ng, P.A. Lee, Phys. Rev. Lett. **61**, 1768 (1988); Y. Meir, N.S. Wingreen, and P.A. Lee, Phys. Rev. Lett. **70**, 2601 (1993).
12. K. G. Wilson, Rev. Mod. Phys. **47**, 773 (1975).
13. H.R. Krishna-Murthy, J.W. Wilkins and K.G. Wilson, Phys. Rev. **B 21**, 1003 (1980).

14. O. Sakai, Y. Shimizu, and T. Kasuya, J. Phys. Soc. Jpn. **58**, 3666 (1989).
15. T.A. Costi, A.C. Hewson, and V. Zlatić, J. Phys.:Cond. Mat. **6**, 2519 (1994).
16. R. Bulla, A.C. Hewson, and Th. Pruschke, J. Phys.: Cond. Mat. **10**, 8365 (1998).
17. W. Hofstetter, R. Bulla, and D. Vollhardt, Phys. Rev. Lett. **84**, 4417 (2000).
18. W. Hofstetter, Phys. Rev. Lett. **85**, 1508 (2000).
19. Walter Hofstetter, *Renormalization Group Methods for Quantum Impurity Systems*, (Shaker, Aachen 2000).
20. R.P. Feynman, *Statistical Mechanics*, Addison Wesley, New York 1972.
21. T.A. Costi, Phys. Rev. Lett. 85, 1504 (2000).
22. A. Yacoby *et al.*, Phys. Rev. Lett. **74**, 4047 (1995); R. Schuster *et al.*, Nature **385**, 417 (1997).
23. D. Loss and E.V. Sukhorukov, Phys. Rev. Lett. **84**, 1035 (2000).
24. D. Boese, W. Hofstetter, and H. Schoeller, preprint cond-mat/0010250.
25. T. Inoshita *et al.*, Phys. Rev. B **48**, 14725 (1993).
26. T. Pohjola *et al.*, Europhys. Lett. **40**, 189-194 (1997).
27. W. Izumida *et al.*, J. Phys. Soc. Jpn. **66**, 717 (1997).
28. W. Izumida *et al.*, J. Phys. Soc. Jpn. **67**, 2444 (1998).
29. M.A. Ruderman and C. Kittel, Phys. Rev. **96**, 99 (1954).
30. W. Hofstetter, to be published.
31. U. Wilhelm and J. Weis, Physica **E6**, 668 (2000).
32. A.W. Holleitner *et al.*, preprint cond-mat/0011044.
33. C. Kergueris, J.-P. Bourgoin, S. Palacin, D. Esteve, C. Urbina, M. Magoga, and C. Joachim, Phys. Rev. **B 59**, 12505 (1999).